Quantum wave packet dynamics of the $1\,^3A''$ $N(^4S)+NO(\tilde{X}\,^2\Pi)$ $\rightarrow N_2(\tilde{X}\,^1\Sigma_g^+)+O(^3P)$ reaction

Pablo Gamallo, Miguel González,[a] and R. Sayós
Department de Química Física i Centre de Recerca en Química Teòrica, Universitat de Barcelona, C/Martí i Franquès 1, 08028 Barcelona, Spain

Carlo Petrongolo[b]
Dipartimento di Chimica, Universita' di Siena, Via A. Moro 2, 53100 Siena, Italy

(Received 23 May 2003; accepted 16 July 2003)

We present the quantum dynamics of the title reaction using the Gray–Balint–Kurti wave-packet (WP) method, several NO vibro-rotational levels, product coordinates, and an asymptotic analysis. We calculate accurate reaction probabilities at $J=0$, estimate those at $J>0$ via a capture model, and discuss the reaction mechanism analyzing the WP time evolution. We also obtain cross sections and rate constants. The potential is barrier-less and thus both probabilities and cross sections do not have a collision-energy ($E_{\rm col}$) threshold. The probabilities present many sharp resonances, due to the $E_{\rm col}$ redistribution on the NNO-internal and N_2-product degrees of freedom. The reaction is stereo-specific and occurs via a bent abstraction mechanism. The cross sections decrease with $E_{\rm col}$, in agreement with the expected behavior for threshold-less reactions. The present values of the rate constant support previous and less accurate calculations, and are in excellent agreement with laboratory experimental data. This confirms the accuracy of the present $1\,^3A''$ PES. © *2003 American Institute of Physics.* [DOI: 10.1063/1.1606672]

I. INTRODUCTION

Recently, some of us investigated theoretically the reaction $N(^4S)+NO(\tilde{X}\,^2\Pi)\rightarrow N_2(\tilde{X}\,^1\Sigma_g^+)+O(^3P)$, the reverse one, and the N-atom exchange reaction on the $1\,^3A''$ and $1\,^3A'$ potential energy surfaces (PESs).[1,2] We calculated more than 10 000 *ab initio* points of these surfaces in Ref. 1, employing the cc-pVTZ Dunning's basis set[3] and the complete active space self-consistent-field and second-order perturbation methods. In Ref. 2, we fitted the *ab initio* PESs to three-body analytical forms and calculated variational-transition-state-theory (VTST) rate constants in a wide temperature range, finding a good agreement with laboratory observed rates.

According to Ref. 2, the reaction $N(^4S)+NO(\tilde{X}\,^2\Pi)$ $\rightarrow N_2(\tilde{X}\,^1\Sigma_g^+)+O(^3P)$ is exoergic by 3.29 eV, does not present any $1\,^3A''$ potential barrier, and has a barrier height of 0.36 eV on the $1\,^3A'$ PES. On the other hand, the N-atom exchange occurs preferentially on the $1\,^3A'$ PES, with a barrier height of 1.19 eV whereas its $1\,^3A''$ barrier height is equal to 1.75 eV. According to these PES features, the title reaction should be the preferred process at collision energies $E_{\rm col}$ smaller than ~1 eV and at temperatures T below ~2000 K. This is shown in Fig. 1, where we plot the $1\,^3A''$ N+NO reactant channel at the equilibrium NO bond length of $2.17\,a_0$. We clearly see that the approaching N atom prefers the N end of the NO diatom and that the minimum energy path (MEP) at $<$NNO$\approx$109° is quite narrow, hinting at a N bent abstraction mechanism with a high steric requirement. On the other hand, both collinear abstraction and insertion mechanisms occur at higher energies.

References 1 and 2 improve considerably previous theoretical studies of the $N(^4S)+NO(\tilde{X}\,^2\Pi)$ system, which employed less accurate *ab initio*[4,5] and semiempirical[6] PESs and quasi-classical trajectory[5–9] (QCT) or reduced quantum approaches.[8] On the other hand, some laboratory rate constants[10–15] are in poor agreement among themselves and are remarkably different from those inferred from models of planetary atmospheres.[16,17] Although previous calculations confirm some laboratory rates, they are based on statistical VTSTs[2] or on a semiempirical PES and QCTs.[6] This paper thus extend previous calculations, presenting an accurate quantum wave packet (WP) study of the title reaction on the $1\,^3A''$ analytical PES of Ref. 2. We describe shortly the method in Sec. II, report reaction probabilities and mechanism in Sec. III, and present cross sections and rate constants in Sec. IV.

In a future work, we shall employ both $1\,^3A''$ and $1\,^3A'$ PESs[2] in a WP study of both N-abstraction and N-exchange reactions: Probabilities and cross sections at higher $E_{\rm col}$, rate constants at higher T, and product vibro-rotational distributions.

II. METHOD

We employ the Gray–Balint–Kurti method[18] that propagates real WPs under an arccos mapping of a shifted and scaled molecular Hamiltonian, via a Chebyshev time-recursion. This method is related to other WP techniques, as the time-independent WP method of Huang *et al.*,[19,20] the Mandelshtam and Taylor's work on Green's function expan-

[a]Electronic mail: m.gonzalez@qf.ub.es
[b]Electronic mail: petrongolo@unisi.it

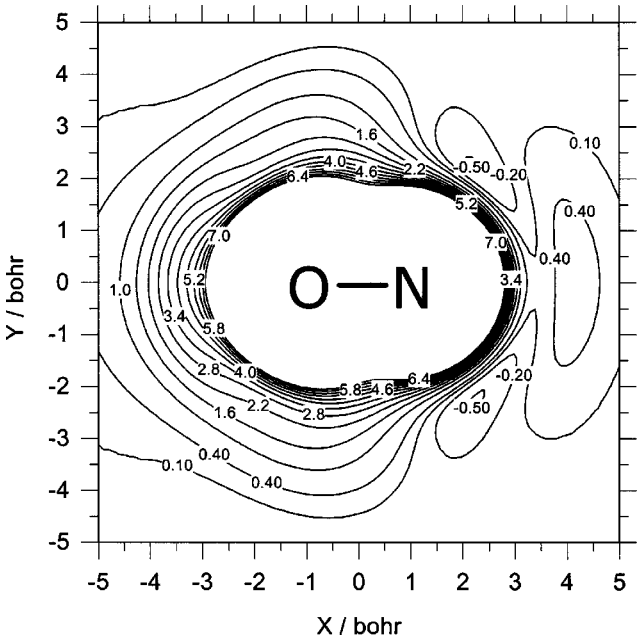

FIG. 1. 1 $^3A''$ PES for $r(\mathrm{NO})=2.17\,a_0$, as function of the (x,y) coordinates of the other N atom. Energy in eV, with respect to $\mathrm{N}+\mathrm{NO}(r_{\mathrm{eq}})$.

sions with damped Chebyshev recursions,[21,22] and it is an extension to scattering processes of the work by Chen and Guo.[23,24]

Using reactant or product coordinates, reaction probabilities are obtained via asymptotic[18] or flux[25] analysis. In this study, the initial WP is defined in reactant Jacobi coordinates R, r, and γ, and is then transformed to the product ones R', r', and γ' for the subsequent time-propagation and asymptotic analysis. We thus take into account the $^{14}N_2$ permutation and nuclear-spin symmetries, which require that $^{14}N_2(^1\Sigma_g^+,v',j')$ vibro-rotational states with $j'=even$ or odd have nuclear statistical weights equal to 2/3 or 1/3, respectively.[26] Reaction probabilities resolved on the vibro-rotational reactant state (v,j) at total angular momentum quantum number J and E_{col} are thus equal to

$$P^J_{vj}(E_{\mathrm{col}})=\sum_{v'}\left\{\frac{2}{3}\left[\sum_{j'=ev}{}^{ev}P^J_{v'j',vj}(E_{\mathrm{col}})\right]+\frac{1}{3}\left[\sum_{j'=od}{}^{od}P^J_{v'j',vj}(E_{\mathrm{col}})\right]\right\}, \tag{1}$$

where ev and od are even and odd j' quanta, respectively, and $P^J_{v'j',vj}$ are state-to-state probabilities.

Accurate probabilities at $J=0$ are calculated for $v=0$ and 1, $j=0-10$ (2), and $E_{\mathrm{col}}\leqslant 1$ eV with the parameters of Table I. A propagation converges the probability in 40 000 steps, requiring ~2.14 CPU days on a Compaq Alpha DS20E/667 work station. On the other hand, probabilities at $J>0$ are estimated via a capture model (CM) following an idea by Gray *et al.*[27] The collision involves indeed three heavy nuclei, and both exact and centrifugal-sudden[28] calculations at $J>0$ are very CPU-time demanding. Because the reaction occurs without potential barrier and the PES is attractive, the present CM assumes that the early dynamics, before product formation, is dominated by the effective potentials

TABLE I. Parameters of the calculations.[a]

Translational energy center of the initial WP	0.4 eV
R center and width of the initial WP	10 and 0.1
R' range and no. of grid points	0–14.5 and 329
r' range and no. of grid points	1.5–16.5 and 197
No. of Legendre polynomials and of γ' points	50 (including potential symmetry)
Potential and centrifugal cutoff	0.44
R' and r' absorption start at	11.5 and 13.5
R' and r' absorption strength	0.01
Asymptotic analysis at R'	8.5

[a]Values in a.u., unless otherwise specified.

$$V^J_{jK}(R)=\min_{r,\gamma}V(R,r,\gamma)+[J(J+1)+j(j+1)-2K^2]/2\mu_R R^2,\quad r\leqslant 2.31\,a_0. \tag{2}$$

Here $V(R,r,\gamma)$ is the PES, K is the projection of J along $\boldsymbol{R}$, μ_R is the reduced mass associated with R, and the upper limit on r avoids the opening of the N_2+O product channel. The second term in the rhs member of Eq. (2) is the centrifugal potential, and these effective potentials present centrifugal barriers that depend on the three quantum numbers. We, therefore, estimate $J>0$ probabilities as

$$P^J_{vjK}(E_{\mathrm{col}})\approx P^0_{vj0}(E_{\mathrm{col}}-E^J_{jK}), \tag{3}$$

where the energy shifts E^J_{jK} are equal to

$$E^J_{jK}=\max_R V^J_{jK}(R)-\max_R V^0_{j0}(R). \tag{4}$$

In Eq. (2) we minimize the PES with respect to r and γ, and for N+NO this is a better choice than Eq. (13) of Ref. 27, because the corresponding $V^J_{jK}(R)$ present only shoulders as functions of J and K. As an example, Fig. 2 shows two effective potentials for $j=8$, $J=0$ or 50, and $K=0$ or 4, respectively. We clearly see the centrifugal barriers at $R=5.11\,a_0$, giving $E^{50}_{8,4}=0.075$ eV, and the minima at -0.758 and -0.565 eV and at $R=3.20\,a_0$.

Initial-state-resolved cross sections $\sigma_{vj}(E_{\mathrm{col}})$ are obtained via the usual partial wave sums,[28] and rate constants $k_{vj}(T)$ and $k(T)$ are calculated as Boltzmann averages[29] in the 100–2000 K range. The thermal rate constant k is obtained by estimating the rates k_{vj} for odd $j\leqslant 9$ with linear interpolations and those for $j\geqslant 10$ via extrapolations, and including[2,6] both spin–orbit (SO) $^2\Pi_{1/2}$ and $^2\Pi_{3/2}$ NO states with their energy difference[30] $\Delta=119.82$ cm^{-1}. Assuming that $^2\Pi_{1/2}$ correlates with the PES, the electronic population is thus equal to

$$p^{el}(T)=\frac{3}{4[2+2\exp(-\Delta/k_BT)]}, \tag{5}$$

where 3 and 4 are the degeneracies of NNO($^3A''$) and N(^4S), respectively, and the second term of the denominator is the NO electronic partition function. Note that $p^{el}(T)$ decreases with T from 3/8 to 3/16.

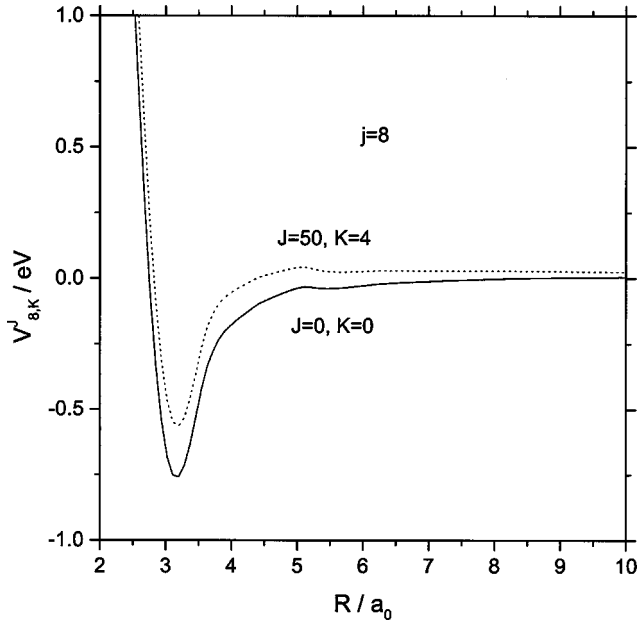

FIG. 2. Effective potentials for $j=8$: $J=0$ and $K=0$ (full line), and $J=50$ and $K=4$ (dotted line). Energy in eV, with respect to N+NO(r_{eq}).

III. REACTION PROBABILITIES AND MECHANISM

Figure 3 shows three examples of reaction probabilities at $J=0$, corresponding to $(v,j)=(0,0)$, (0,8), and (1,0). Note that the (0,8) vibro-rotational level of NO is that most populated at room T among those here considered, and that the j' even and odd sums of Eq. (1) are nearly equal. The use of this equation is, therefore, not necessary in the present reaction.

The $1\,^3A''$ PES is without a reaction barrier, and thus the probabilities do not present an energy threshold and their average values increase from very low E_{col} up to 1 eV. The probabilities are dominated by strong Feshbach resonances over the full energy range, i.e., the collision energy is transformed into internal energy owing to the minima of the effective potentials or the large reaction exoergicity. The role of the effective potentials should be more important at low E_{col}, when the centrifugal minima can trap part of the WP giving rise to quasi-bound NNO states and to a collision-to-internal energy redistribution. Because the sharpest resonance is that of $P^0_{0,8}$ at $E_{col}=0.015$ eV, with a full width at half maximum of $\sim$69 cm^{-1}, the lifetimes of these collision complexes should be as large as $\sim$77 fs.

At higher collision energy, these resonances are probably due to the opening and closing of several N_2 vibro-rotational product channels, owing to the flow of the collision energy of the approaching N atom into these N_2 modes.

Note also that the NO rotational excitation enhances the reaction probabilities, mainly at low collision energy, whereas the NO vibrational excitation has a little effect on the reactivity. As in Refs. 27 and 31, we explain these (v,j) effects analyzing the effective interaction-centrifugal potentials

$$V^{\text{int-cent}}_{vj}(R)=\langle \phi^{\text{NO}}_{vj}(r)L_j(\gamma)|V(R,r,\gamma) - V^{\text{NO}}(r)|\phi^{\text{NO}}_{vj}(r)L_j(\gamma)\rangle_{r\gamma}+j(j+1)/2\mu_R R^2, \tag{6}$$

where ϕ^{NO}_{vj} and L_j are NO states and normalized Legendre polynomials, respectively. The barriers of these potentials are in general lower increasing the NO j quanta, showing that this probability enhancement is due to a lower effective interaction potential [first term of the rhs member of Eq. (6)] in spite of the increase of the second centrifugal term. There-

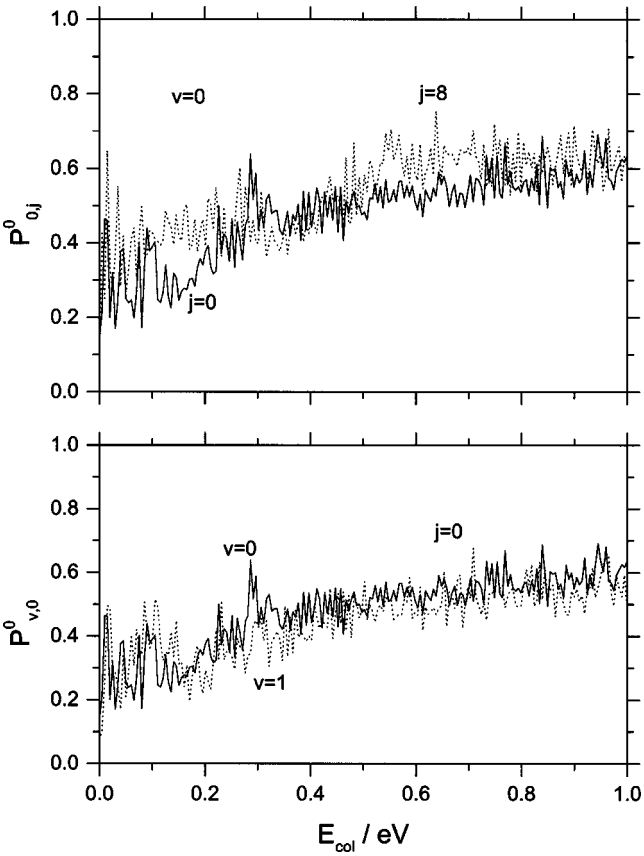

FIG. 3. Reaction probabilities at $J=0$. Above: $v=0$, and $j=0$ (full line) and 8 (dotted line). Below: $j=0$, and $v=0$ (full line) and 1 (dotted line).

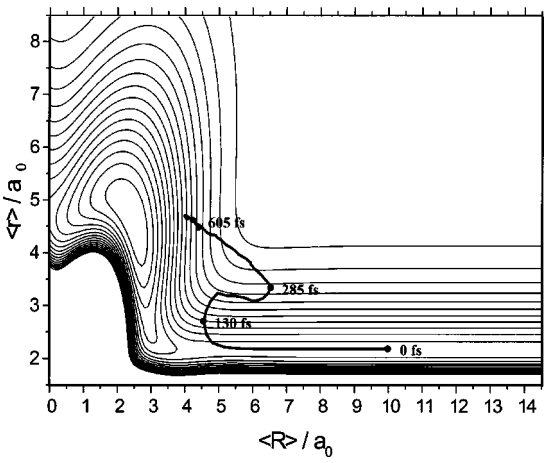

FIG. 4. Radial trajectory for $v=0$ and $j=8$, superimposed on the plot of the PES at $\gamma=50°$. Time in fs and energy in eV with respect to N+NO(r_{eq}). The PES outermost line is at 6 eV and the lines are spaced by 0.57 eV, so that the innermost line is at -2.55 eV.

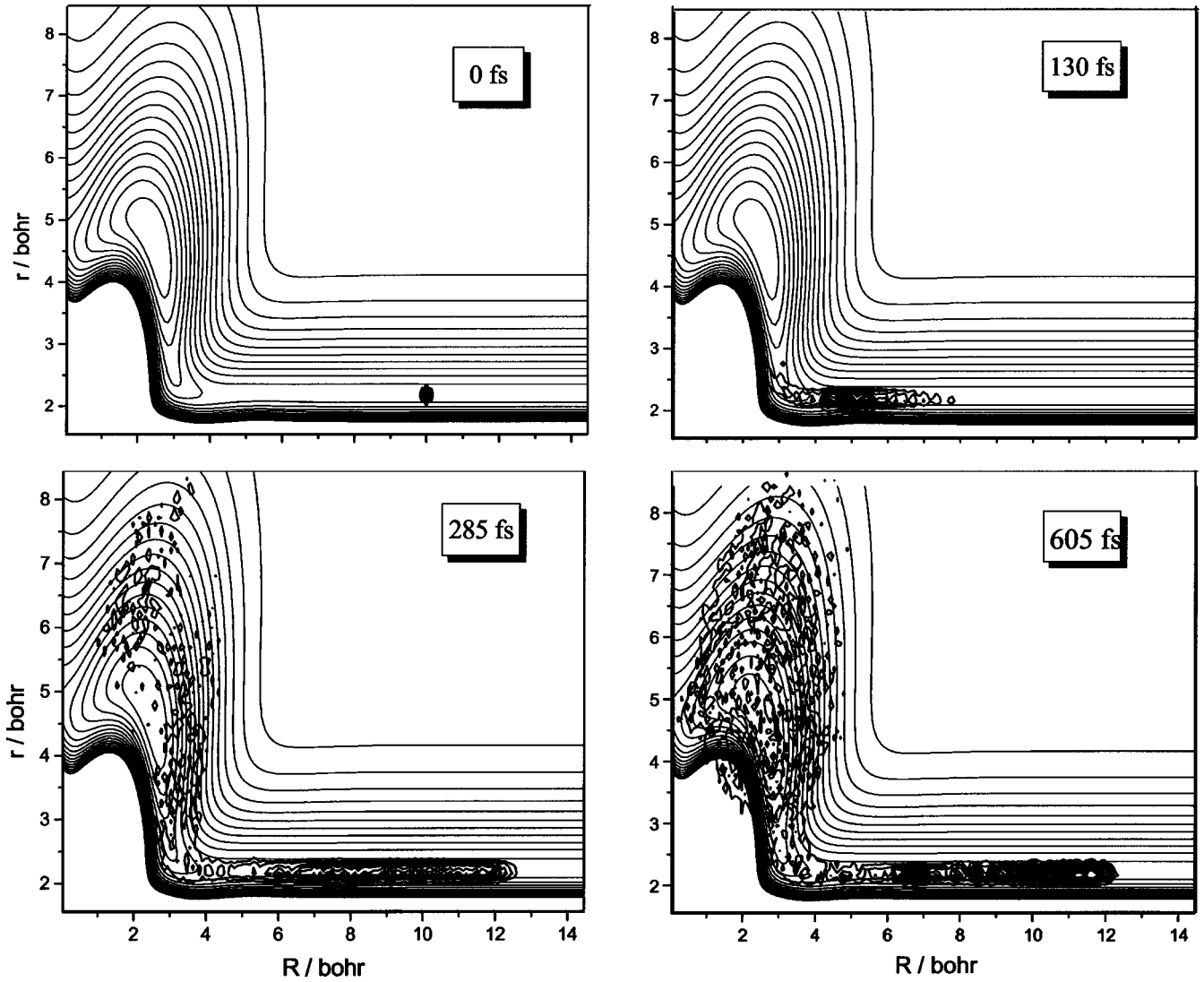

FIG. 5. γ-averaged WP density for $v=0$ and $j=8$. See the Fig. 4 caption for further details.

fore, stereo-specific effects due to proper alignment of the N atoms along the MEP, and inferred from Fig. 1, overcome the larger centrifugal barrier.

As for $N+O_2$,[32] expectation values of the reactant coordinates $\langle R\rangle$, $\langle r\rangle$, and $\langle\gamma\rangle$, and snapshots of the WP at various times give qualitative insights into the reaction mechanism. We thus plot in Fig. 4 the radial trajectory and in Fig. 5 the γ-averaged probability density for $(v,j)=(0,8)$ at 0, 130, 285, and 605 fs. These results are superimposed on the plot of the PES at $\gamma=50°$ whose deep hole corresponds to a part of the N_2+O product channel. In the first ~100 fs, the WP moves in a narrow N+NO reactant channel, reaching the interaction region with $\langle r\rangle$ nearly unperturbed. This confirms the role of the mutual orientation of the reactants we mentioned by discussing Fig. 1 and Eq. (6). Between ~130 and ~285 fs, the repulsive wall of the PES reflects back part of the WP towards the reactant channel, and both $\langle R\rangle$ and $\langle r\rangle$ increase. At larger times, part of the WP eventually enters the N_2+O product channel and spreads on a wide (R,r) space, whereas $\langle r'(N_2)\rangle$ decreases. On the overall, the WP density is negligible at $R\approx 0$, and $\langle\gamma\rangle$ decreases from 90° at 0 fs up to ~60° at the end of the reaction. This is a quantum description of a bent abstraction mechanism, which can be contrasted with the $H_2+O(^1D)$ insertion reaction.[33]

It is useful to contrast this reaction with that similar between N and O_2,[31] which was investigated with the same method here employed, has $\tilde{X}\,^2A'$ and $\tilde{a}\,^4A'$ reaction barriers of 0.30 and 0.65 eV, and is exoergic by 1.41 eV. Owing to the potential barriers, the $N+O_2$ probabilities have collision energy thresholds that depend on the initial (v,j) level of O_2 and decrease in general at high j, and the probability resonances are less sharp than the present ones, owing to the smaller exoergicity.

IV. CROSS SECTIONS AND RATE CONSTANTS

Figure 6 shows that the cross sections for $(v,j)=(0,0)$, (0,8), and (1,0) decrease as the collision energy increases from ~0.015 to ~0.20–0.40 eV, depending on the initial NO rotational level. This is consistent[29] with a barrierless reaction and with a long-range potential $V(R)\approx -C_s/R^s$ that dominates the dynamics at low $E_{\rm col}$. For example, a linear fit to $\log(\sigma_{0,8}/\text{Å}^2)$ for $0.015<E_{\rm col}<0.40$ eV, gives

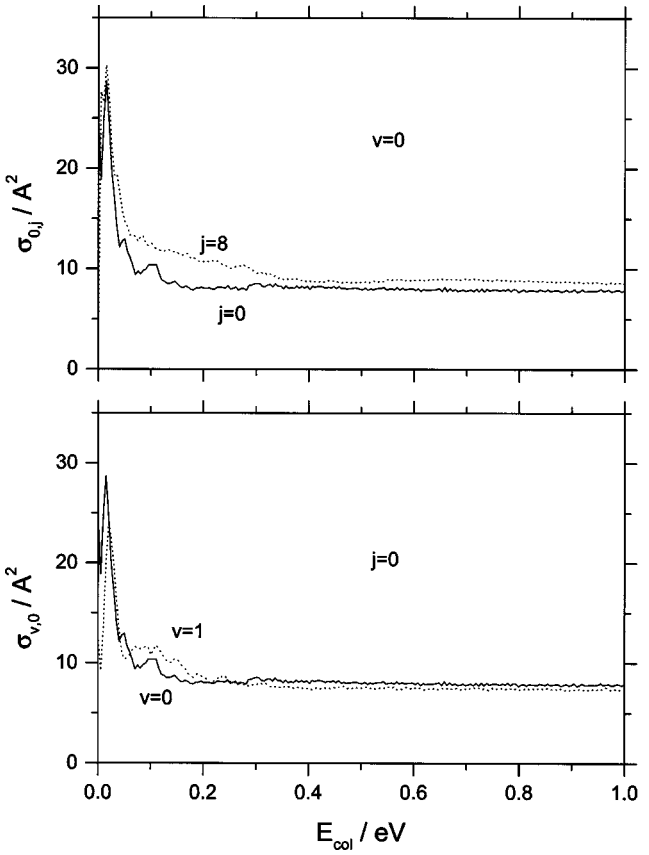

FIG. 6. Cross sections. Above: $v=0$, and $j=0$ (full line) and 8 (dotted line). Below: $j=0$, and $v=0$ (full line) and 1 (dotted line).

$$\log \sigma_{0,8}(E_{\mathrm{col}}) = (0.82 \pm 0.01) - (0.30 \pm 0.01) \log E_{\mathrm{col}}, \qquad (7)$$

with standard deviation equal to 0.03. From this equation and from Eq. (2.58) of Ref. 29, we estimate that $s \approx 6.67$, and $C_s \approx 1.58\,\mathrm{eV} \times \mathrm{Å}^{6.67}$.

Increasing the collision energy, the cross sections become nearly constant because more N_2+O product channels are now opened. At low E_{col} and j, some cross-section resonances survive the partial wave sum, with $\sigma_{0,0} < \sigma_{0,8}$ and $\sigma_{0,0} \approx \sigma_{1,0}$, in agreement with the probability results.

The WP initial-state-resolved cross sections are rather similar to the $^3A''$ one of Ref. 9. However, the agreement is quite fortuitous because σ of Ref. 9 was obtained via a semiempirical PES, using a QCT method and a Boltzmann distribution at 500 K of the NO vibro-rotational states. Unlike the N+NO results, the $N+O_2$ cross sections[31] are zero up to a threshold energy and increase with E_{col}, like the reaction probabilities and owing to the potential barriers.

Figure 7 shows initial-state-resolved rate constants $k_{vj}(T)$ at 300 and 2000 K as functions of the NO(v,j) quanta. They oscillate somewhat with j, with a minimum at $j=2$, are rather constant at high j, save $k_{1,j}(300)$ that decreases, and are reduced by v, mainly at 300 K and high j. Moreover, these rates increase moderately with T (up to about two times for $k_{1,10}$), because in their expression[29] the decrease of σ with E_{col} reduces the enhancement of the Boltzmann factor with T. This behavior is due to the absence of any potential barrier and reaction threshold, and is very different from that of $N+O_2$.[31] Owing to the $\tilde{X}\,^2A'$ and $\tilde{a}\,^4A'$ potential barriers of the latter reaction, its $k_{vj}(T)$ are indeed orders of magnitude smaller and are very sensitive to the $O_2(v,j)$ level at room T and to the temperature.

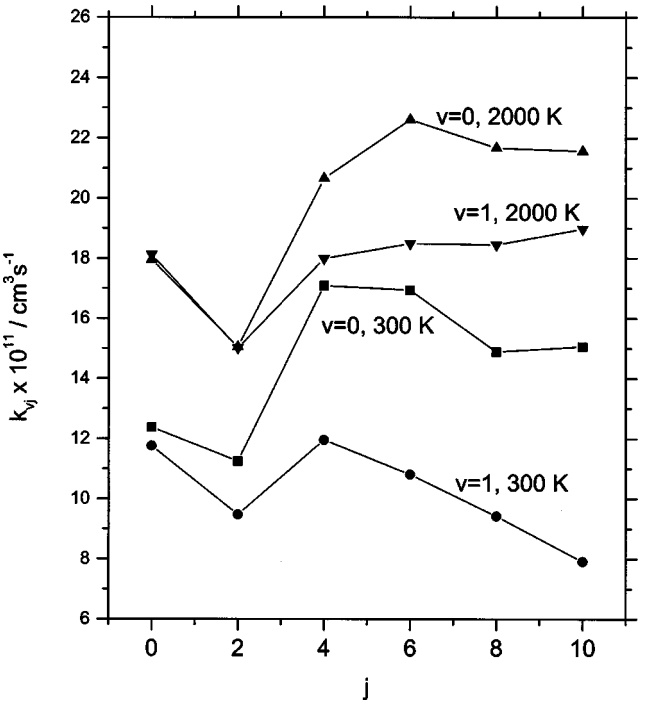

FIG. 7. Initial-state-resolved rate constants at 300 and 2000 K.

Table II and Fig. 8 contrast the calculated WP and ICVT/μ OMT-SO[2] thermal rate constants $k(T)$ with the experimental recommended[14,15] and laboratory[10,12] values between 100 and 2000 K. The reviews of Refs. 14 and 15 are based on other laboratory data.[11,13] The experimental rates are given as upper and lower bounds in Table II and as analytical fits of the data in Fig. 8. WP rates in $\mathrm{cm^3 s^{-1}}$ were also calculated in this temperature range in steps of 100 K and best-fitted to the equation

$$k(T) = A T^x \exp(B/T), \qquad (8)$$

finding $A = (1.15 \pm 0.06) \times 10^{-11}$, $x = 0.15 \pm 0.01$, and $B = 79.97 \pm 3.99$. Note the small value of x and the negative value of the ''activation'' energy.

Because the reaction occurs without a collision energy threshold, k varies very few with T, even less than the initial-state-resolved k_{vj} do, decreasing by ~16% from 100 up to 600 K, and then increasing by only ~9% up to 2000 K. The behavior up to 600 K is due to the decrease of the electronic population p^{el} of Eq. (5), because omitting this term the rate increases in the full T range, from $13.04 \times 10^{-11}\,\mathrm{cm^3 s^{-1}}$ at 100 K to $19.48 \times 10^{-11}\,\mathrm{cm^3 s^{-1}}$ at 2000 K. The subsequent change of slope at higher T reflects the moderate increase of k_{vj} shown in Fig. 7. The low and high T behaviors of the rate constant are described by the exponential and T^x terms of Eq. (8), respectively.

We see that the WP and ICVT/μ OMT-SO[2] rates are in qualitative agreement in the full temperature range, although they are somewhat quantitatively different. Indeed, for $T \leqslant 300$ K the statistical rate seems too large, and the opposite holds above 600 K where it changes slope at ~1000 K. Note

TABLE II. Theoretical WP and VTST rate constants $k\times10^{11}$ in cm^3s^{-1}, versus experimental recommended and laboratory upper and lower bounds.

T/K	WP	VTST[a]	Recomm.[b]	Recomm.[c]	Lab.[d]	Lab.[e]
100	4.15					
200	3.87	6.52	2.3–5.4		2.4–4.6	
300	3.65	4.68	2.2–3.8			1.2–3.7
400	3.54	3.79	1.9–3.8			1.8–4.6
600	3.49	3.20				2.8–5.9
1000	3.61	3.05				
1500	3.77	3.11		2.7–6.7		
2000	3.81	3.29		3.0–7.6		

[a]Reference 2, ICVT/μ OMT-SO, including both 1 $^3A''$ and 1 $^3A'$ PESs.
[b]Reference 15.
[c]Reference 14.
[d]Reference 12. The rate is constant in the full temperature range.
[e]Reference 10.

that the weight of the excited 1 $^3A'$ PES to the thermal rate constant is negligible up to 2000 K, where it is maximal and equal to 7%.[2] The WP rates confirm those QCT calculated in Ref. 6 up to 1000 K, when Eq. (5) is employed,[2] although the PESs and the theoretical treatments are quite different as we mentioned above.

Like previous and less accurate calculations,[2,6] the WP rate is in excellent agreement with laboratory[11–13] and recommended[14,15] values, in particular with the constant value of Ref. 12. Note also that the theoretical error bounds of Eq. (8) are lower than the experimental ones. On the other hand, both the present results and those of Refs. 2, 6, 11–15 do not support the oldest experimental value.[10] As in Refs. 2 and 6, the WP rate is different from those inferred in models of planetary atmospheres,[16,17] so that these models are uncorrect and/or the planetary populations of the reactants are different from the laboratory thermal one.[6] The comparison with the $N+O_2$ $k(T)$[31] confirms the very different behavior of the initial-state-resolved rates of these two reactions. In conclusion, these WP results point out the accuracy of the present 1 $^3A''$ PES.

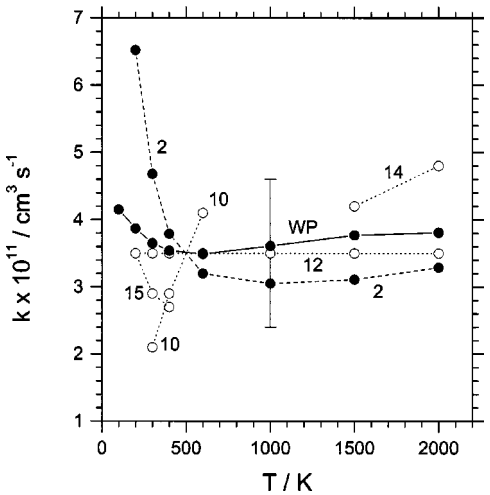

FIG. 8. Thermal rate constants. Calculated: WP (full line) and ICVT/μ OMT-SO (dashed line with ref. number) with full circles. Experimental: Dotted lines with ref. numbers and open circles. Reference 12 with the error bar. See Table II for other experimental error bars.

ACKNOWLEDGMENTS

We thank Dr. S. K. Gray and P. Defazio for many discussions, suggestions, and assistance. P.G. thanks the Universities of Barcelona and Siena for pre-doctoral research grants. This work was supported by the Spanish Ministry of Science and Technology (Projects BQU2002-03351 and BQU2002-04269-C02-02), by MIUR, University of Siena, and IPCF-CNR of Pisa, Italy.

[1] P. Gamallo, M. González, and R. Sayós, J. Chem. Phys. **118**, 10602 (2003).
[2] P. Gamallo, M. González, and R. Sayós, J. Chem. Phys. **118**, 2545 (2003).
[3] T. H. Dunning, Jr., J. Chem. Phys. **90**, 1007 (1989).
[4] S. P. Walch and R. L. Jaffe, J. Chem. Phys. **86**, 6947 (1987).
[5] M. Gilibert, A. Aguilar, M. González, F. Mota, and R. Sayós, J. Chem. Phys. **97**, 5542 (1992).
[6] J. W. Duff and R. D. Sharma, Geophys. Res. Lett. **23**, 2777 (1996).
[7] M. Gilibert, A. Aguilar, M. González, and R. Sayós, J. Chem. Phys. **99**, 1719 (1993).
[8] A. Aguilar, M. Gilibert, X. Giménez, M. González, and R. Sayós, J. Chem. Phys. **103**, 4496 (1995).
[9] J. W. Duff and R. D. Sharma, Chem. Phys. Lett. **265**, 404 (1997).
[10] M. A. A. Clyne and I. S. McDermid, J. Chem. Soc. Faraday Trans. **71**, 2189 (1975).
[11] J. H. Lee, J. V. Michael, W. A. Payne, and L. J. Stief, J. Chem. Phys. **69**, 3069 (1978).
[12] J. V. Michael and K. P. Lim, J. Chem. Phys. **97**, 3228 (1992).
[13] P. O. Wennberg, J. G. Anderson, and D. K. Weisenstein, J. Geophys. Res. **99**, 18839 (1994), and references therein.
[14] D. L. Baulch, C. J. Cobos, R. A. Cox *et al.*, J. Phys. Chem. Ref. Data **23**, 847 (1994), and references therein.
[15] W. B. DeMore, S. P. Sander, C. J. Howard, A. R. Ravinshankara, D. M. Golden, C. E. Kolb, R. F. Hampson, M. J. Kurylo, and M. J. Molina, in *Chemical Kinetics and Photochemical Data for Use in Stratospheric Modeling*, Evaluation 12, NASA-JPL, Publication 97-4 (Pasadena, CA, 1997), and references therein.
[16] D. E. Siskind and D. W. Rusch, J. Geophys. Res. **97**, 3209 (1992).
[17] J. L. Fox, J. Geophys. Res. **99**, 6273 (1994).
[18] S. K. Gray and G. G. Balint-Kurti, J. Chem. Phys. **108**, 950 (1998).
[19] Y. Huang, D. J. Kouri, and D. K. Hoffman, J. Chem. Phys. **101**, 10493 (1994).
[20] Y. Huang, S. S. Iyengar, D. J. Kouri, and D. K. Hoffman, J. Chem. Phys. **105**, 927 (1996).
[21] V. A. Mandelshtam and H. S. Taylor, J. Chem. Phys. **102**, 7390 (1995).
[22] V. A. Mandelshtam and H. S. Taylor, J. Chem. Phys. **103**, 2903 (1995).
[23] R. Chen and H. Guo, J. Chem. Phys. **105**, 3569 (1996).
[24] R. Chen and H. Guo, Chem. Phys. Lett. **261**, 605 (1996).
[25] A. J. H. Meijer, E. M. Goldfield, S. K. Gray, and G. G. Balint-Kurti, Chem. Phys. Lett. **293**, 270 (1998).

[26] G. Herzberg, *Molecular Spectra and Molecular Structure* (Krieger, Malabar, Florida, 1989), Vol. I, p. 134.
[27] S. K. Gray, G. G. Balint-Kurti, G. C. Schatz, J. J. Lin, X. Liu, S. Harich, and X. Yang, J. Chem. Phys. **113**, 7330 (2000).
[28] R. T. Pack, J. Chem. Phys. **60**, 633 (1974).
[29] R. D. Levine and R. B. Bernstein, *Molecular Reaction Dynamics and Chemical Reactivity* (Oxford University Press, New York, 1987), pp. 179 and 59.
[30] K. P. Huber and G. Herzberg, *Molecular Spectra and Molecular Structure* (Van Nostrand, New York 1979), Vol. IV, p. 476.
[31] P. Defazio, C. Petrongolo, C. Oliva, M. González, and R. Sayós, J. Chem. Phys. **117**, 3647 (2002).
[32] P. Defazio, C. Petrongolo, S. K. Gray, and C. Oliva, J. Chem. Phys. **115**, 3208 (2001).
[33] S. K. Gray, C. Petrongolo, K. Drukker, and G. C. Schatz, J. Phys. Chem. A **103**, 9448 (1999).